Comparison of Backbone Dynamics of Oxidized and Reduced Putidaredoxin by ^{15}N NMR Relaxation Measurements

Neşe Sari, Marcia J. Holden, Martin P. Mayhew, Vincent L. Vilker, and Bruce Coxon*

Biotechnology Division, National Institute of Standards and Technology, Gaithersburg, Maryland 20899

Received March 19, 1999; Revised Manuscript Received June 1, 1999

ABSTRACT: The backbone dynamics of uniformly ^{15}N-labeled reduced and oxidized putidaredoxin (Pdx) have been studied by 2D ^{15}N NMR relaxation measurements. ^{15}N T_1 and T_2 values and $^1H-^{15}N$ NOEs have been measured for the diamagnetic region of the protein. These data were analyzed by using a model-free dynamics formalism to determine the generalized order parameters (S^2), the effective correlation time for internal motions (τ_e), and the ^{15}N exchange broadening contributions (R_{ex}) for each residue, as well as the overall correlation time (τ_m). Order parameters for the reduced Pdx are generally higher than for the oxidized Pdx, and there is increased mobility on the microsecond to millisecond time scale for the oxidized Pdx, in comparison with the reduced Pdx. These results clearly indicate that the oxidized protein exhibits higher mobility than the reduced one, which is in agreement with the recently published redox-dependent dynamics studied by amide proton exchange. In addition, we observed very high T_1/T_2 ratios for residues 33 and 34, giving rise to a large R_{ex} contribution. Residue 34 is believed to be involved in the binding of Pdx to cytochrome P450cam (CYP101). The differences in the backbone dynamics are discussed in relation to the oxidation states of Pdx, and their impact on electron transfer. The entropy change occurring on oxidation of reduced Pdx has been calculated from the order parameters of the two forms.

Putidaredoxin (Pdx)[1] is a 106-residue protein that occurs naturally in the soil bacterium *Pseudomonas putida* (*1*). It belongs to a family of ferredoxins that have a single Fe_2S_2 cluster. Pdx mediates electron transfer between the NADH-dependent flavoprotein Pdx-reductase and P450cam in the camphor hydroxylation reaction, while cycling between the oxidized ($Fe^{3+}-Fe^{3+}$) and the reduced ($Fe^{3+}-Fe^{2+}$) forms. The structure of Pdx and its dependence on the redox state have been extensively studied by Pochapsky and co-workers. Despite the paramagnetism of the metal cluster, a solution structure model was derived by using mainly proton-detected NMR methods (*2*). Certain subtle structural differences were seen to exist between the reduced and oxidized forms of Pdx. These differences suggest the existence of a more rigid structural framework in the vicinity of the Fe-S cluster in the case of reduced Pdx (*3*). The redox dependences of the hyperfine-shifted ^{13}C and ^{15}N resonances of putidaredoxin have been described recently (*4*).

Our interest lies in the structure and function of Pdx and its electron-transfer properties in relation to the redox state. Since minimal changes occur in the protein architecture as a function of oxidation state, it would be worthwhile to ascertain the dynamic properties of Pdx in this context. This study relates the role of Pdx dynamics to its function as an electron carrier. Recently, a redox-dependent dynamics study by amide proton exchange showed that there is a decrease in protein dynamics upon reduction, particularly in regions adjacent to the metal cluster (*5*). Protein dynamics studies by amide exchange give valuable information about the events occurring on a slower time scale (milliseconds to hours); they are mostly rotation of buried side chains, and local unfolding/folding. However, it is important to investigate the events on different time scales to improve our understanding of the dynamic changes in Pdx with respect to its oxidation state. Therefore, we have investigated the ^{15}N backbone dynamics of Pdx as a function of its oxidation state, where the motions studied are in the picoseconds to nanoseconds time scale. These include concerted motions of several atoms, rotation of surface side chains, and torsional vibrations or relative motions of domains. In addition, motions on a slower time scale (microseconds to milliseconds) can be recognized as ^{15}N line broadening contributions arising from conformational exchange. Here, we present a study of the backbone dynamics of uniformly ^{15}N-labeled reduced and oxidized Pdx by 2D ^{15}N NMR relaxation measurements. T_1, T_2, and $^1H-^{15}N$ NOE values have been measured for the *diamagnetic* regions of the proteins. Our measurements of ^{15}N T_1 values for the *paramagnetic* regions of oxidized and reduced Pdx have been reported previously (*6*, *7*). The data for the diamagnetic region have been analyzed by using a model-free dynamics formalism (*8*) to determine the generalized order parameters (S^2), the effective correlation time for internal motions (τ_e), and the ^{15}N exchange broadening contributions (R_{ex}) for each residue,

* Corresponding author: National Institute of Standards and Technology, 100 Bureau Dr., Stop 8311, Gaithersburg, MD 20899-8311. Fax: 301-975-5449. Telephone: 301-975-3135. E-mail: bruce.coxon@nist.gov.

[1] Abbreviations: 2D, two-dimensional; NOE, nuclear Overhauser enhancement; Pdx, putidaredoxin; NADH, nicotinamide adenine dinucleotide reduced form; DNase, deoxyribonuclease; DEAE, diethylaminoethyl; DTT, 1,4-dideoxy-1,4-dithio-DL-threitol; HSQC, heteronuclear single quantum correlation.

10.1021/bi9906423
Published on Web 07/15/1999

as well as the overall correlation time (τ_m). The results are compared with other dynamics studies of Pdx, and a general picture for the redox-dependent dynamic changes is discussed.

Although similar dynamic changes have been observed in the heme proteins cytochrome *c* and cytochrome b_5 (*9*, *10*), this is the first study to delineate the backbone dynamics of an Fe-S protein as a function of its redox state.

EXPERIMENTAL PROCEDURES

Sample Preparation. Pdx protein was heterologously expressed in *E. coli* (DH5α) from a plasmid (pRE1) containing the gene for Pdx under control of the λP_L promoter. The cells were transformed with a second plasmid (pRK248) containing the gene for the temperature-sensitive C1587λ repressor. The cells were initially grown in batch culture in a rich broth at 32 °C, a temperature at which there was no expression of Pdx, followed by harvesting in mid-log phase. The cells were then transferred to a defined medium with $^{15}NH_4Cl$ (Cambridge Isotopes,[2] $^{15}N > 98$ atom %) as the sole source of nitrogen. Cell growth was continued at 39 °C (a permissive temperature for expression), and the cells were harvested 5 h later. Pdx protein was purified according to Grayson et al. (*11*). In short, the cells were lysed by freeze−thaw, followed by the addition of lysozyme and DNase. The cell debris was removed by centrifugation, and Pdx was then purified by two chromatographic steps. The protein was first eluted from a DEAE Fast Flow Sepharose column with a KCl gradient, which was followed by a gel filtration column. The purity of the final protein was >99%. Prior to use in NMR experiments, the purified protein was exchanged with a buffer containing 5 mmol/L phosphate (pH 7.4), 0.01% NaN_3, and 1 mmol/L DTT. The protein was concentrated to 3.5 mmol/L and purged with argon prior to analysis. For the preparation of reduced Pdx, oxidized Pdx was extensively purged with argon, and then reduced with excess dithionite in a nitrogen glovebox. During the NMR experiments, screw-cap, argon-filled 5 mm NMR tubes were used for both the oxidized and the reduced samples.

NMR Spectroscopy. NMR experiments were performed by use of a Bruker AMX-500 spectrometer for the T_1 and T_2 experiments, and a Bruker DRX-500 for the NOE measurements. All experiments were conducted at 290 K, using 3.5 mmol/L solutions of the oxidized and reduced forms of Pdx.

^{15}N T_1 and T_2 measurements were performed by using 2D $^1H-^{15}N$ HSQC experiments (*12*) with water flip-back (*13*) and Watergate (*14*) modifications for water suppression. For the T_1 and T_2 experiments, a recycle delay of 1.5 s was used between acquisitions to ensure sufficient recovery of ^1H magnetization. For T_1 experiments, 12 variable delays were used (20.5, 41.0, 82.0, 163.8, 327.6, 655.2, 982.9, 1310.5, 1638.1, 1965.7, 2293.3, 2629.5 ms), and for T_2 experiments, 10 variable delays were used (7.5, 22.4, 52.4, 82.3, 112.2, 142.1, 172.0, 231.9, 291.7, 351.6 ms). T_1 and T_2 values were calculated by nonlinear, least-squares fitting of the cross-peak heights to a single-exponential decay, and Monte Carlo simulations were performed to estimate the uncertainties (*15*).

$^1H-^{15}N$ NOEs were measured by using $^1H-^{15}N$ correlation spectra with a gradient-selected, sensitivity-enhanced pulse sequence (*16*). A relaxation delay of 4 s prior to a 4 s proton presaturation period was employed for the experiments with NOE, and presaturation was applied 4 MHz off-resonance with the same recycling delay, for the experiments without NOE. The NOEs were calculated as the ratios of peak heights in the spectrum recorded with proton saturation to those in the spectrum recorded without saturation. The mean NOEs and standard uncertainties were calculated from four independent measurements.

For all the experiments, the spectral width in F_2 was 8064 Hz and the ^1H carrier was set on the water signal; the spectral width in F_1 was 5600 Hz and the ^{15}N carrier was set to 118 ppm. T_1 and T_2 experiments were acquired using 128 × 1024 complex points and a total of 32 scans per t_1 point. NOE experiments were collected as 144 × 1024 complex point data sets with 16 scans per t_1 point.

Data Analysis. Spectra were processed using FELIX version 95.0 (Biosym Technologies, San Diego, CA). A $\sin^2$ function shifted by $\pi/2$ rad was used in the direct and indirect dimensions, and fids were zero-filled once in both dimensions. Relaxation data were extracted from Felix 95.0 by relaxation scripts, and analyzed by use of the Modelfree (version 3.1) software package provided by Dr. Arthur Palmer III, Department of Biochemistry and Molecular Biophysics, Columbia University, New York, NY. All the processing and analyses were done with a Silicon Graphics Indigo 2 R10000 work station.

The relaxation of an amide ^{15}N nucleus is dominated by dipolar interaction with the directly attached NH proton, and by chemical shift anisotropy (*17*). The T_1 and T_2 relaxation times and the NOE values are then described by eqs 1−3:

$$1/T_1 = (1/4)d_{NH}^2[J(\omega_H - \omega_N) + 3J(\omega_N) + 6J(\omega_H + \omega_N) + c^2J(\omega_N)] \quad (1)$$

$$1/T_2 = (1/8)d_{NH}^2[4J(0) + J(\omega_H - \omega_N) + 3J(\omega_N) + 6J(\omega_H) + J(\omega_H + \omega_N)] + (c^2/6)[4J(0) + 3J(\omega_N)] + R_{ex} \quad (2)$$

$$\mathrm{NOE} = 1 + (d_{NH}^2T_1/4)(\gamma_H/\gamma_N)[6J(\omega_H + \omega_N) - J(\omega_H - \omega_N)] \quad (3)$$

where $d_{NH} = (\mu_o h/8\pi^2)/\gamma_H\gamma_N r_{NH}^{-3}$, $c = \omega_N\Delta\sigma/3^{1/2}$, $\mu_o = 4\pi \times 10^{-7}$ T·m·A^{-1} is the permeability of free space, $h = 6.626 \times 10^{-34}$ J·s is Planck's constant, $\gamma_H = 26.7522 \times 10^7$ s^{-1}·T^{-1} and $\gamma_N = -2.7108 \times 10^7$ s^{-1}·T^{-1} are the gyromagnetic ratios of ^1H and ^{15}N, respectively, $r_{NH} = 1.02$ Å is the nitrogen−proton bond length, $\omega_H = 2\pi$ rad × 500.13 MHz and $\omega_N = 2\pi$ rad × 50.68 MHz are the Larmor frequencies of the ^1H and ^{15}N nuclei, respectively, and $\Delta\sigma = -160$ ppm is the chemical shift anisotropy measured for ^{15}N nuclei in helical polypeptide chains (*18*). The R_{ex} term in eq 2 is the ^{15}N exchange broadening term, which affects the transverse relaxation rates due to chemical exchange, or other pseudo-first-order processes.

[2] Certain commercial equipment, instruments, or materials are identified in this paper to specify adequately the experimental procedure. Such identification does not imply recommendation by the National Institute of Standards and Technology, nor does it imply that the materials are necessarily the best for the purpose.

The motions and their time scales within the protein can be determined from the relaxation data by a model-free formalism developed by Lipari and Szabo (*19, 20*) and extended by Clore and co-workers (*21*). This formalism uses a number of parameters to describe the spectral density function, which defines the motion of a certain nucleus in the protein observed by NMR:

$$J(\omega) = 2/5\{[S^2\tau_m/(1 + (\omega\tau_m)^2)] + [(1 - S_f^2)\tau'_f/(1 + (\omega\tau'_f)^2)] + [(S_f^2 - S^2)\tau_s/(1 + (\omega\tau'_s)^2)]\} \quad (4)$$

where $\tau'_f = \tau_f\tau_m/(\tau_f + \tau_m)$, $\tau'_s = \tau_s\tau_m/(\tau_m + \tau_s)$, τ_m is the rotational correlation time of the entire molecule, τ_f is the effective correlation time for internal motions on a fast time scale ($\tau_f < 100-200$ ps), τ_s is the effective correlation time for internal motions on a slow time scale ($\tau_f < \tau_s < \tau_m$), $S^2 = S_f^2S_s^2$ is the square of the generalized order parameter, and S_f^2 and S_s^2 are the squares of the order parameters for the motions on the fast and the slow time scales, respectively. The overall tumbling of the molecule is assumed to be isotropic; the principal components of the inertial tensor as calculated from the NMR structure of Pdx (*2, 3*) appear to be in the approximate ratio of 0.7:0.9:1.0, indicating that the overall motion is unlikely to be significantly anisotropic. The order parameter S^2 describes the degree of spatial restriction of the internal motion of the $^{15}N-^{1}H$ bond vector. The order parameter takes values from 0 for isotropic internal motions to 1 if the motion is totally restricted to the molecular frame. The order parameter is used to describe motions in the picoseconds to nanoseconds time scale, whereas conformational exchange processes, which can be deduced from R_{ex} terms, are within the microseconds to milliseconds time scale.

Calculation of model-free parameters from the measured relaxation rate constants and NOEs was performed by minimizing the sum of the squared residuals between the experimental and calculated values (*8*).

Model Selection. The model selection outlined by Palmer and co-workers (*8*) was used to select an appropriate model for the fitting of each residue. An average T_1/T_2 ratio was calculated for the backbone amides, and an initial estimate of τ_m was obtained from this average value (*12*). A grid search was then used to obtain initial estimates for the values of the other model-free parameters. Five dynamic models consisting of subsets of the extended model-free parameters were initially fitted to each residue using the fixed value of τ_m estimated from the T_1/T_2 ratios. In each case, 500 randomly distributed, calculated data sets were generated using Monte Carlo simulations to estimate the probability distributions for statistics characterizing the goodness-of-fit (within a 95% confidence limit) between the dynamic models and the experimental data.

The dynamic models are based on optimizing the following parameters: (1) S^2; (2) S^2, $\tau_e = \tau_f$; (3) S^2, R_{ex}; (4) S^2, $\tau_e = \tau_f$, R_{ex}; and (5) S_f^2, S^2, $\tau_e = \tau_s$. In model 1, it is assumed that $S_s^2 = 1$ and $\tau_f \rightarrow 0$; i.e., slow motions are negligible, and fast motions are very fast (<20 ps). In model 2, it is assumed that $S_s^2 = 1$; i.e., slow motions are negligible, and fast motions ($\tau_f < 100-200$ ps) are detectable. Model 3 has the conditions of model 1, and an additional chemical exchange term is calculated for a particular residue. Model 4 includes a chemical exchange term, in addition to τ_f. In model 5, it is assumed that fast and slow motions are distinguishable. Since models 4 and 5 cannot be treated statistically, a different approach was taken in choosing these models, as defined by Mandel et al. (*8*).

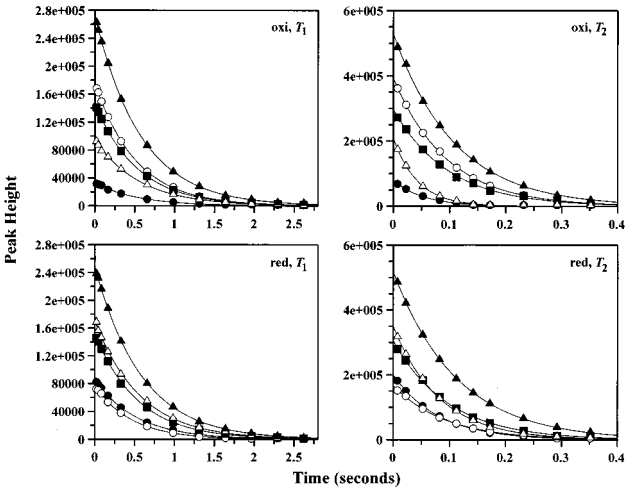

FIGURE 1: Examples of T_1 (left panels) and T_2 (right panels) relaxation curves for some residues of the oxidized (oxi) and reduced (red) Pdx. The curves represent the best fits to single-exponential decays. Experimental data points for Tyr33 (open triangles), Asp34 (closed circles), Val60 (closed triangles), Ile89 (open circles), and Trp106 (closed squares) are shown. Error bars are smaller than the size of the characters used to indicate the data points.

RESULTS

The ^{15}N resonance assignments and correlation with backbone ^{1}H assignments for the oxidized and reduced Pdx have been reported previously (*5*). However, only 75% of the total amide NH correlations could be made, because of the paramagnetic broadening of the peaks around the Fe_2S_2 center. In this study, 65 out of 106 amide resonances of Pdx were resolved sufficiently well for accurate peak height measurements in the T_1, T_2, and NOE experiments to be made for both the oxidized and reduced forms. The difficulty in resolving the rest was mainly due to spectral overlap within the diamagnetic region.

Relaxation Parameters. Single-exponential, two-parameter decay curves were fitted to the T_1 and T_2 decay data, and χ^2 values indicated that all 65 residues were adequately fitted by the two-parameter decay curves, for both the oxidized and the reduced Pdx. Plots of the experimental data points and the decay curves obtained from the fitting procedure for several residues are shown in Figure 1.

For both the oxidized and the reduced Pdx, the values of the relaxation parameters T_1, T_2, and NOE are summarized in Figure 2. The average values and their uncertainties are listed in Table 1. Although there is almost no difference between the average values for the oxidized and reduced forms, 66% of the T_1 values are shorter, and 60% of the NOE values are smaller in the oxidized form than in the reduced form.

Trp106 Side-Chain NH Group. The relaxation data for the side-chain indole NH group of Trp106 were analyzed similarly to those of the backbone amide groups. The T_1, T_2, and NOE values are listed in Table 2 as a comparison

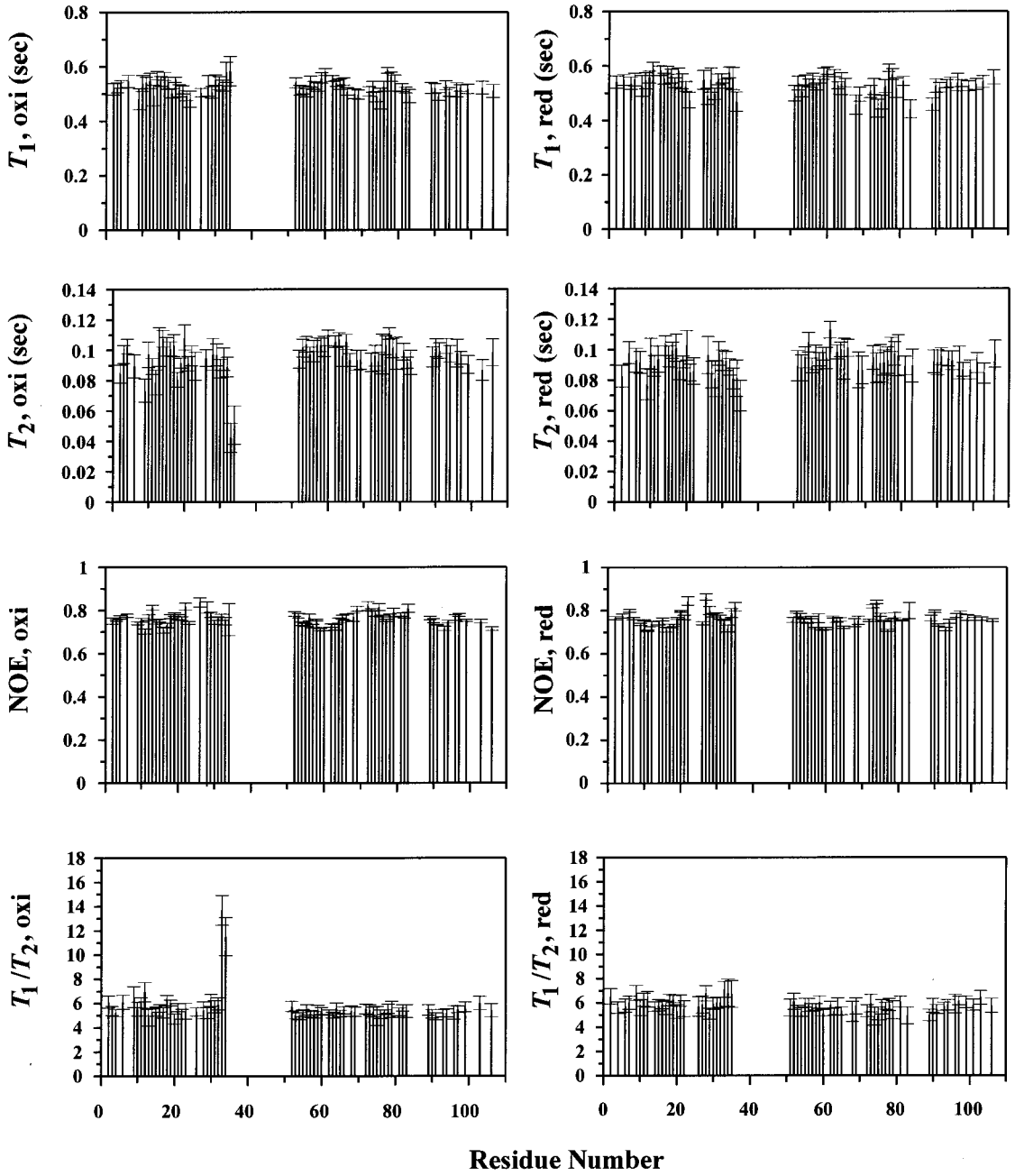

FIGURE 2: T_1, T_2, $^1H-^{15}N$ NOE, T_1/T_2 ratios, and uncertainties are plotted for the spectrally resolved backbone NH groups in the oxidized (left panels) and reduced (right panels) Pdx as a function of residue number. T_1 and T_2 data were obtained by fitting the measured peak heights to a single exponential as described by Palmer et al. *(15)*. NOE values and their uncertainties are the averages and the standard uncertainties, respectively, of the values determined for each of four data sets.

Table 1: Average Values of ^{15}N Relaxation Parameters[a] for Putidaredoxin at 17 °C and 500 MHz

	oxidized Pdx	reduced Pdx
$\langle T_1 \rangle_{ave}$ (s)	0.53 ± 0.02	0.53 ± 0.03
$\langle T_2 \rangle_{ave}$ (s)	0.096 ± 0.007	0.092 ± 0.009
$\langle T_1/T_2 \rangle_{ave}$	5.48 ± 0.44	5.78 ± 0.43
$\langle NOE \rangle_{ave}$	0.76 ± 0.03	0.76 ± 0.03

[a] The average T_1, T_2, $^1H-^{15}N$ NOE, and T_1/T_2 ratios and the overall average standard uncertainties for the spectrally resolved backbone NH groups in the oxidized and reduced Pdx.

between the side-chain and backbone NH groups. The relaxation data were included in the model-free analyses described below using a chemical shift anisotropy of −89 ppm (*22*).

Estimation of the Overall Correlation Time τ_m. Under conditions where the internal motions are less than 100 ps, the molecular correlation time is greater than 1 ns, and T_2 is not shortened significantly by chemical exchange, the ratio T_1/T_2 is considered to be independent of the order parameters of the residues or the internal motions, and provides an initial estimate of the overall molecular correlation time τ_m (*12*, *21*). Omitting the data with unusually high or low T_1 and T_2 values, the average T_1/T_2 ratio was used to estimate τ_m as 8.0 ns for the oxidized, and 8.3 ns for the reduced Pdx. The difference between the two τ_m's is not significant enough to indicate dimerization of Pdx in the reduced state. An earlier study on the redox-dependent dynamics of Pdx characterized by amide exchange also did not show evidence for dimer-

Table 2: Relaxation and Dynamic Parameters for Tryptophan 106 Side-Chain and Backbone NH Groups[a]

parameter	oxidized	reduced
	Side-Chain NH Group	
T_1 (s)	0.59 ± 0.02	0.61 ± 0.02
T_2 (s)	0.126 ± 0.008	0.129 ± 0.007
NOE	0.68 ± 0.01	0.70 ± 0.01
T_1/T_2	4.67	4.73
$S^2_{sidechain}$	0.79 ± 0.03	0.79 ± 0.02
τ_e (ps)	37.2 ± 6.2	31.5 ± 5.8
	Backbone NH Group	
T_1 (s)	0.53 ± 0.02	0.56 ± 0.02
T_2 (s)	0.098 ± 0.009	0.097 ± 0.008
NOE	0.71 ± 0.01	0.75 ± 0.01
T_1/T_2	5.43	5.75
$S^2_{backbone}$	0.88 ± 0.04	0.88 ± 0.03
τ_e (ps)	54.1 ± 19.7	25.5 ± 8.5

[a] Shown are the measured relaxation parameters (T_1, T_2, $^1H-^{15}N$ NOE) and T_1/T_2 ratios, and the calculated dynamic parameters (S^2, τ_e) and their standard uncertainties for the side-chain and the backbone NH groups of Trp106. The R_{ex} term was not selected for optimization for either the backbone or the side-chain NH groups.

ization in either of the two oxidation states at a 3.5 mmol/L concentration (*5*).

Model-Free Analysis. A selection criterion based on the analysis of T_1/T_2 ratios can be applied to determine whether an exchange contribution to the apparent transverse relaxation rate of the nitrogen spins or an effective internal motion can be detected (*21*). Internal motion (τ_f <100−200 ps) can be detected if the T_1/T_2 ratio is more than one standard deviation below the mean, and the R_{ex} term can be included if the T_1/T_2 ratio is more than one standard deviation above the mean. The T_1/T_2 ratios for Pdx are plotted in Figure 2 for both oxidation states. Residues Arg13, Gly20, Glu54, Ala63, Thr75, and Thr91 in the oxidized Pdx and residues Gly20, Ser29, Glu54, Val60, Ile68, Val74, Thr75, Arg83, and Ile89 in the reduced Pdx have T_1/T_2 ratios which are more than one standard deviation below the mean. This indicates that an effective internal motion can be detected for these residues. Therefore, model 2 is the appropriate choice for them. Additionally, model 2 turned out to be the statistically chosen dynamic model for these residues. Residues Lys2, Val6, Asp9, Thr11, Arg12, Ala18, Asp19, Asn30, Ile32, Tyr33, Asp34, and Asp103 in the oxidized form and residues Lys2, Asp9, Thr11, Arg12, Ala18, Asp19, Val28, Tyr33, Asp34, and Asp103 in the reduced Pdx have T_1/T_2 ratios that are more than one standard deviation above the mean. Even though T_1/T_2 ratios indicated R_{ex} terms for almost the same residues for each oxidation state, model 3 was statistically chosen only for two residues (Tyr33 and Asp34) for the reduced Pdx, and the other amide groups displayed negligible (~ 0 s^{-1}) R_{ex} terms. In contrast, the R_{ex} term was included in either model 3 or model 4 for each of the aforementioned residues of the oxidized Pdx. Additionally, the most striking difference in the T_1/T_2 ratios is seen in amide groups Tyr33 and Asp34 of the oxidized Pdx. The T_1/T_2 ratios of these two residues are much higher than those of other residues in the oxidized Pdx, and this large difference in the T_1/T_2 ratios is not seen in the reduced Pdx.

Relaxation data for each residue were analyzed by using spectral density functions using one or more parameters (model 1 to model 5) with fixed τ_m values initially estimated from the T_1/T_2 ratios (*8*). All residues could be fitted adequately to one of the dynamic models, and it was not necessary to choose model 5 for any residue in either oxidation state of Pdx. A final calculation was performed by optimizing τ_m for the whole molecule, using the appropriate models chosen for each residue. Table 3 shows the average order parameters, optimized τ_m's, and distributions of the residues among the five models applied for both the oxidized and the reduced Pdx. Plots of the optimized values of the model-free parameters for the backbone resonances of each oxidation state are shown in Figure 3.

Table 3: Dynamic Parameters Optimized in the Final Model-Free Analysis[a]

	oxidized Pdx	reduced Pdx
no. of resonances in calculation	65	65
model 1 (S^2 optimized)	21	20
model 2 (S^2, τ_e optimized)	34	44
model 3 S^2, R_{ex} optimized)	3	2
model 4 (S^2, τ_e, R_{ex} optimized)	7	0
model 5 (S_f^2, S^2, τ_e optimized)	0	0
$\langle S^2\rangle_{ave}$	0.89 ± 0.03	0.93 ± 0.03
optimized τ_m (ns)	8.00 ± 0.04	8.31 ± 0.05

[a] Shown is a summary of the input relaxation parameters and optimized dynamic parameters in the final model-free calculations for the oxidized and reduced Pdx; parameters were selected for optimization using the criteria discussed in the text. The average order parameters ($\langle S^2\rangle_{ave}$ ± standard uncertainty) and the optimized rotational correlation time (τ_m ± standard uncertainty) are also listed.

Generalized Order Parameter, S^2. The mean value of the order parameter for reduced Pdx, $\langle S^2_{red}\rangle_{ave}$, is higher than the mean value of the order parameter for oxidized Pdx, $\langle S^2_{oxi}\rangle_{ave}$ (see Table 3). Although the difference between the average order parameters barely exceeds the uncertainties, $S^2_{red} > S^2_{oxi}$ for 44 residues, $S^2_{red} \sim S^2_{oxi}$ for 10 residues, and $S^2_{red} < S^2_{oxi}$ for 7 residues. The differences between the order parameters for the residues of the reduced and the oxidized forms are shown in Figure 4.

Effective Correlation Time, τ_e. A total of 44 amide nitrogens in the reduced form and 41 amide nitrogens in the oxidized form exhibit detectable effective internal motion. The τ_e's of the amide nitrogens in the reduced form are generally longer than the τ_e's observed for the oxidized form. However, the differences in the amplitudes of the internal motions for each oxidation state are more-or-less within the standard uncertainties in τ_e values, and there is no pronounced difference in terms of the amplitudes of these internal motions.

Conformational Exchange Parameter, R_{ex}. Optimization on the amide nitrogens of the oxidized form required R_{ex} terms for 13 residues of this form, but for only 2 residues of the reduced form. These 13 residues in the oxidized Pdx are also the ones identified by the R_{ex} terms obtained from the T_1/T_2 ratios. The two residues in the reduced form are Tyr33 and Asp34, which have R_{ex} terms 2.91 ± 1.07 and 2.36 ± 1.01 s^{-1}, respectively. Residues Tyr33 and Asp34 in the oxidized Pdx exhibit R_{ex} terms of 14.47 ± 5.52 and 10.57 ± 3.06 s^{-1}. Certainly, the exchange processes are much faster in the oxidized Pdx for these two residues.

DISCUSSION

Absence of Paramagnetic ^{15}N Relaxation in the Diamagnetic Region. An interesting question is whether the ^{15}N

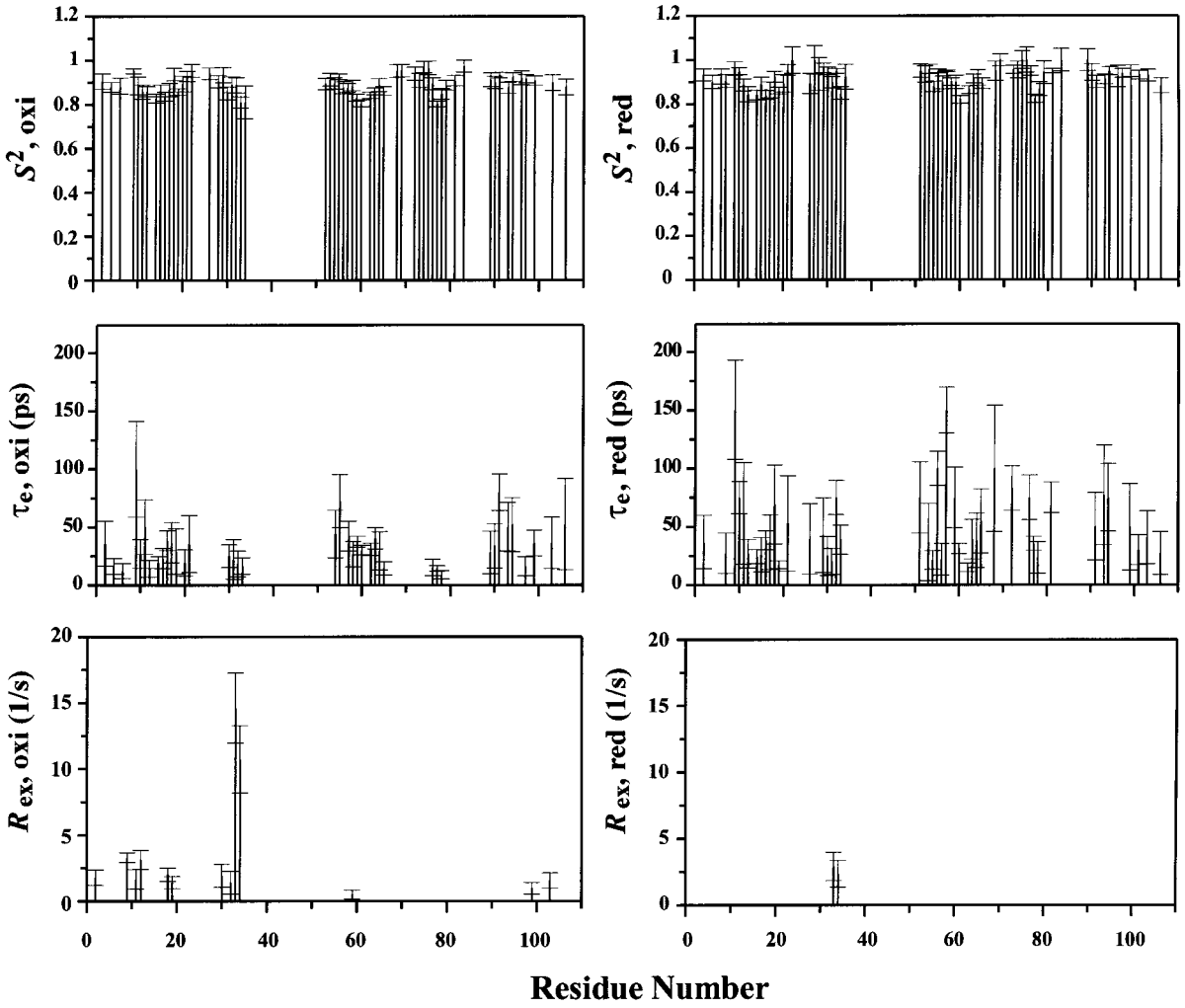

FIGURE 3: Calculated dynamic parameters (S^2, τ_e, R_{ex}) and standard uncertainties are plotted for the spectrally resolved backbone NH groups in the oxidized (left panels) and reduced (right panels) Pdx. Data obtained by fitting the relaxation data shown in Figure 2 to eqs 1−4, according to the criteria discussed in the text.

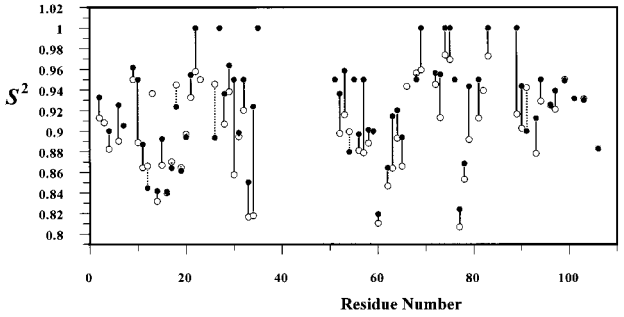

FIGURE 4: Calculated order parameters (S^2) as a function of residue number of the reduced (closed circles) and the oxidized (open circles) Pdx. The S^2 values for the oxidized and reduced forms are connected by solid lines when $S^2_{oxi} < S^2_{red}$, and by dotted lines when $S^2_{oxi} > S^2_{red}$. Most of the residues exhibit lower order parameters in the oxidized state ($S^2_{oxi} < S^2_{red}$) indicating more backbone mobility. No data could be measured for residues Ser7, Ala27, Ile35, Tyr51, and Val101 of the oxidized form, and Val3, Arg13, Leu23, Arg66, and Ser82 of the reduced form.

relaxation parameters measured for the diamagnetic regions of the Pdx proteins are affected by the paramagnetism of the iron−sulfur cluster. In our experience, there is a fairly sharp boundary between the ^{15}N magnetic properties of the paramagnetic and diamagnetic domains of these proteins, as implied in previous discussions (*6*, *7*). At distances from the center of the Fe_2S_2 cluster that are greater than ∼4 Å, paramagnetic relaxation is dominated by the electron−nuclear, dipole−dipole mechanism for both the longitudinal (T_1) and transverse (T_2) relaxation processes. Since the rates of both of these processes are inversely proportional to the sixth power of the distance, the effectiveness of this mechanism falls off very rapidly with distance, and previously, we indicated ∼4−7 Å as the effective range of paramagnetic dipolar relaxation (*6*, *7*). In the present work, we have studied only the diamagnetic region of the protein, which lies outside this effective range. This region is precisely that in which the ^1H relaxation times are long enough to permit evolution of the $^{15}N-^1H$ spin coupling magnetization vectors, thus allowing operation of the inverse detection methods for measurement of T_1 and T_2. Therefore, it may be asserted that the paramagnetic relaxation contribution is negligible in the diamagnetic region, which comprises the majority of the amino acid residues. Strong support for this view comes from previous measurements on the gallium analogue of Pdx (*23*). This metalloprotein is entirely diamagnetic, and at the same NMR frequency as we used for our measurements, this protein has shown (*23*) average ^{15}N T_1 values of ∼0.5 s that are of the same order as the values we have found for the oxidized and reduced iron forms

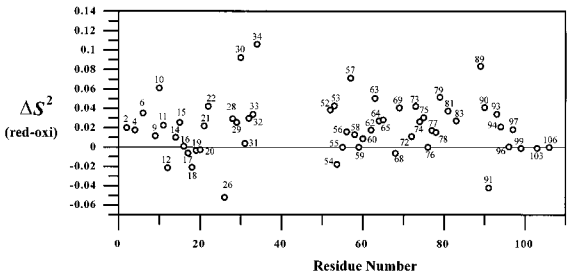

FIGURE 5: Differences in the calculated order parameters between the reduced and the oxidized Pdx [ΔS^2(red−oxi)] as a function of residue number. The positive ΔS^2(red−oxi) values indicate slower backbone dynamics in the reduced state in comparison with the dynamics in the oxidized state of Pdx. The residue numbers are indicated for each point. The largest difference in backbone dynamics as a function of oxidation state is seen in residue 34.

of Pdx. This close agreement supports the assertion that the paramagnetic contribution to ^{15}N relaxation is negligible in the diamagnetic regions of the Pdx proteins studied.

Backbone Dynamics. The average order parameters are larger for the reduced Pdx as compared with the oxidized form (Table 3). Although the differences between the two average order parameters are almost within the error limits, 72% of the amide resonances analyzed by the model-free formalism demonstrated order parameters which were greater for the reduced form than for the oxidized form, while 16% have similar order parameters. The remaining 12% exhibited order parameters that are smaller in the reduced state. Figure 5 shows the differences in the order parameters between the oxidized and the reduced states, ΔS^2(red−oxi). The positive ΔS^2(red−oxi) values indicate faster backbone dynamics in the oxidized state. Figure 6 illustrates the backbone mobility in the oxidized Pdx; the most mobile regions are colored red, regions fairly mobile are colored green, and regions showing slower backbone dynamics are colored blue.

The lowest order parameters are observed in residues Tyr33, Asp34, Val60, and Glu77 in the oxidized Pdx (Figure 4). Tyr33 and Asp34 are at the very beginning of the loop that surrounds the Fe-S center (Figure 6). This region has been found to be important in the binding of Pdx to P450cam. The relevance of our backbone dynamics results and the Pdx binding to P450cam will be discussed in the next section. Residues Glu77 and Leu78 also demonstrate high backbone flexibility, and they are located in the region of the protein termed the C-terminal cluster of Pdx (*2, 3*). The C-terminal cluster of Pdx is comprised of residues that are close to the carboxyl terminus (Pro102−Trp106, Val74−Asn82). It is a compact region defined by a network of interresidue hydrogen bonds (such as side chains of His49, Tyr51, and Ser82), and C-terminal cluster resonances show the largest chemical shift changes upon reduction. The order parameters are higher in the reduced form for residues Glu77, Leu78, Lys79, and Asn81, indicating that reduced Pdx has lower backbone mobility in this region. Val60 is located at the C-terminus of helix F and at the start of a loop region comprised of residues Ala62−Asn64 that shows considerable backbone flexibility in the oxidized protein (Figure 6). The backbone dynamics slow in this loop region upon reduction; however, Val60 is the most mobile residue for both oxidation states. The loop regions comprised by residues Gly10, Asp34, Ala63, Lys79, and Ile89 and the helical regions including residues Asn30 and Thr57 exhibit the highest differences in the order parameters due to a change of oxidation state (Figure 5). Asn30 is in the D helix from which a surface loop starts surrounding the Fe-S center, and Thr57 is in helix F along with Val60 (Figure 6). The differences in the backbone flexibilities as a function of oxidation state in almost every region of the protein indicate that there is a decrease in mobility all over the protein upon reduction.

Although there are no significant changes in the detectable effective internal motions when the results for the two oxidation states are compared, there is more microsecond to millisecond time scale motion in the oxidized form than in the reduced state (Figure 3). The residues that exhibit increased microsecond to millisecond time scale mobility in the oxidized state are in the β-sheets, A and B (Lys2, Val6, Thr11, Arg12), and in the loop regions (Asp9, Ala18, Asp19, Thr91), and also in regions closer to the Fe-S center (Ile32, Tyr33, Asn30, Ile32, Asp34, D103). R_{ex} contributions are around 1−3 s^{-1}. However, R_{ex} contributions for Y33 and D34 (14.5 and 10.6 s^{-1}) are much higher than for the rest of the residues mentioned before, and this will be discussed in the following section. In the reduced state, only two residues, Y33 and D34, displayed an observable R_{ex} contribution (2.9 and 2.4 s^{-1}). This exemplifies the fact that the oxidized state has higher mobility.

Although residues much closer to the paramagnetic center cannot be observed by the 2D methods that are necessary for the measurement of the ^{15}N relaxation parameters, the diamagnetic region of the spectrum demonstrates that there is an overall decrease in the backbone dynamics upon reduction of Pdx. This overall reduction in mobility is distributed all over the protein, as can be observed from the order parameters and increased microsecond to millisecond time scale mobility in the oxidized state. However, one must note that the most drastic changes occur in the regions that are closer to the Fe-S center.

Residue Aspartate 34. Aspartate 34 is contiguous to the surface loop that surrounds the Fe-S center (Figure 6). Site-directed mutagenesis studies have shown that D38, D34, and Trp106 are important for the interaction of Pdx with P450cam. D38 is the most important residue in both electron transfer and binding, while Trp106 and D34 are important in binding only (*24*). A model for the structure of the Pdx−P450cam complex has been proposed based on molecular dynamics simulations, electrostatic calculations, and electron-transfer pathways (*25, 26*). In this model, D38 (Pdx) and R112 (P450cam), D34 (Pdx) and R109 (P450cam), and Trp106 (Pdx) and R79 (P450cam) form three ionic pairs. Therefore, it is important to delineate the dynamic parameters of these residues in Pdx as a function of redox state. Trp106 will be discussed separately in the next section. Unfortunately, D38 cannot be observed by heteronuclear correlation experiments since it is close to the Fe-S center, and its NMR signal is paramagnetically broadened. However, D34 is in the diamagnetic region of the spectrum, and it is possible to study the backbone dynamics of this residue. Interestingly, the largest difference in the order parameters of the two oxidation states is seen in residue D34 ($S^2_{red} = 0.92$, $S^2_{oxi} = 0.82$); i.e., D34 exhibits much more restricted backbone flexibility in the reduced state than it does in the oxidized state (Figure 5). In addition, a large R_{ex} value is also observed for D34 and its neighbor Y33 in the oxidized state, and the R_{ex} contribution is much larger in the oxidized state than it

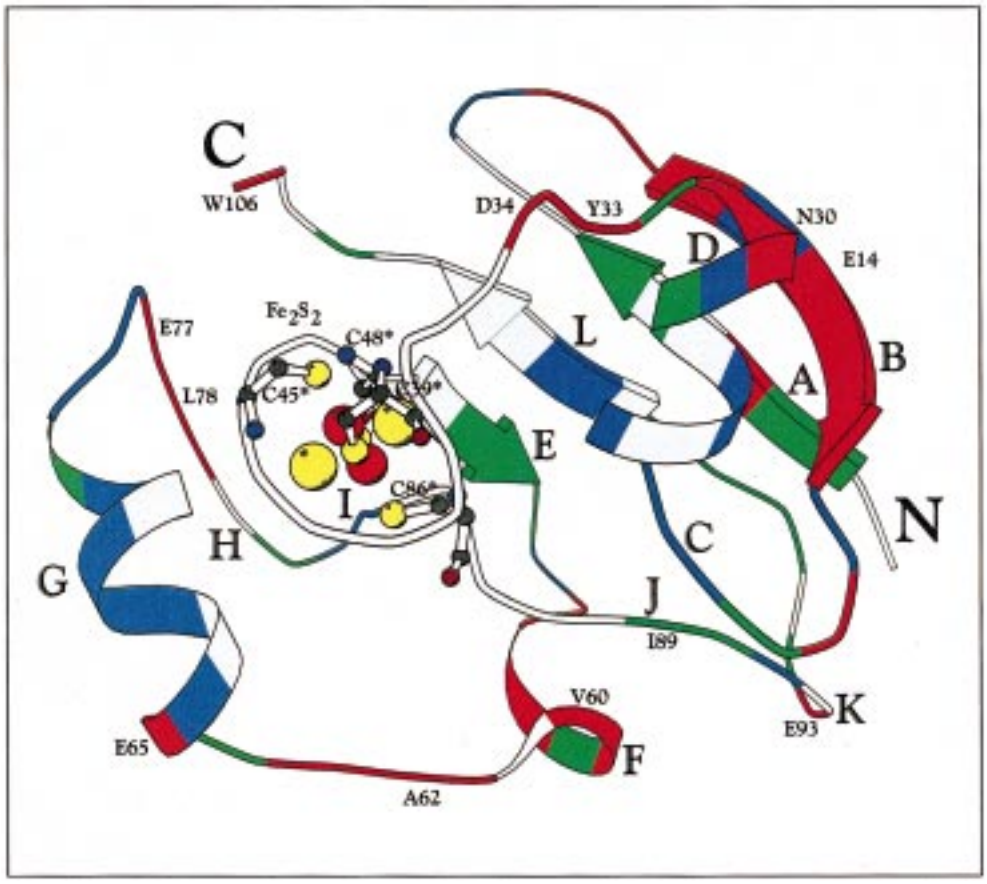

FIGURE 6: Ribbon diagram of the NMR structure of the oxidized Pdx (*2*) showing the relative mobility of the sites and the Fe-S center (C39*, C45*, C48*, and C86* indicating the iron−ligand cysteine residues). The color coding for the ribbons is as follows: red, most mobile ($S^2 < 0.89$); green, moderately mobile ($0.93 > S^2 > 0.89$); blue, restricted backbone motion ($1 > S^2 > 0.93$). Gray indicates residues for which no dynamic parameters were obtained, because of either paramagnetic broadening or spectral overlap.

is in the reduced state (Figure 3). This shows that there is increased microsecond to millisecond scale motion that reflects upon the higher mobility of residues D34 and Y33 in the oxidized state.

The drastic change in the order parameters upon reduction and in the observed microsecond to millisecond time scale motion of D34 which is particularly important in the binding of the two proteins suggests that a tighter binding of the reduced Pdx to P450cam might occur in comparison with the binding of oxidized Pdx. It has already been observed that reduced Pdx has a greater affinity for binding to P450cam than does oxidized Pdx (*27*).

Residue Tryptophan 106. Putidaredoxin contains a single tryptophan residue at its carboxyl terminus (Trp106). Site-directed mutagenesis studies have demonstrated that an aromatic amino acid side chain is required at this position for efficient electron transfer to occur in the physiological Pdx−P450cam complex (*28, 29*). Recently, additional site-directed mutagenesis studies have emphasized that modification of the carboxyl terminus perturbs the binding interaction of Pdx with P450cam, but has no impact on the electron transfer (*24, 27*). Both molecular dynamics simulations (*30*) and steady-state fluorescence experiments (*31*) have demonstrated that Trp106 is solvent-exposed; it rotates free of global protein constraints, and occupies several conformational states with lifetimes in the nanosecond and subnanosecond time scales. Fluorescence experiments were conducted as a function of the redox state. An overall correlation time of 11 ns was estimated for Pdx by using the Stokes−Einstein equation, and a correlation time of 5 ns for the tryptophan motion described by three conformational states. These conformational substates were characterized by three lifetimes (0.2, 2, and 5 ns), with similar relative proportions in both oxidized and reduced putidaredoxin.

Our results, including both the ^{15}N backbone dynamics and side-chain dynamics of Trp106, do not show significant differences when both oxidation states are compared (Table 2). The order parameters are similar for the oxidized and the reduced states. Motions represented by the generalized order parameter are on the picosecond to nanosecond time scale; however, if the τ_e is close to τ_m, a motion independent of the overall tumbling of the molecule may not be recognized by the model-free analysis. Since the motion observed for the indole ring of Trp106 by fluorescence experiments is in the nanosecond time scale, and it is also very close to the overall tumbling motion of the protein, it cannot be identified by ^{15}N dynamics of proteins.

The ratio of the amide proton exchange rates for Trp106 in the oxidized vs reduced Pdx is unity, indicating that the dynamics of Trp106 do not change with respect to its oxidation state (*5*). The results of three different dynamics studies on Trp106, namely, the fluorescence experiments, the amide exchange dynamics, and the ^{15}N backbone and side-chain dynamics, lead to a similar conclusion, indicating that there are no major differences in the dynamics of Trp106 as a function of redox state. This is different from the results

obtained for the other residues in Pdx. There are redox-dependent dynamic differences for most of the residues in Pdx, with an emphasis on the residues closer to the Fe-S center. Because Trp106 dynamics are the same in both oxidized and reduced Pdx, we conclude that the rapid unrestrained motion of the Trp106 side chain is not related to the increase in affinity of reduced Pdx for the cytochrome as compared with oxidized Pdx.

In light of the fact that the redox state dependent dynamics of Pdx were studied in the absence of P450cam, any conformational change that might occur due to the formation of the Pdx−P450cam complex cannot be addressed by investigating the isolated Pdx redox states. Preliminary NMR titrations of oxidized Pdx with P450cam have shown that many NH resonances are affected, most of them being the ones that correspond to the surface-exposed and/or C-terminal cluster residues (*25*). The indole peak of Trp106 is among the resonances perturbed by complexation with P450cam. However, interpretation of these affected resonances is not yet complete.

Comparison with Amide Exchange Dynamics. The dynamics of Pdx have been studied by amide proton exchange (*5*). Amide proton exchange rates are a measure of local solvent accessibility, and provide information about protein dynamics on a slower time scale (milliseconds to hours). The motions that are represented on this time scale are more related to local fluctuations of the protein structure, resulting in exposure of amide protons initially buried in the protein interior, and/or involved in hydrogen bonding interactions (*32, 33*). Amide exchange rates clearly indicate that there is a decrease in protein dynamics upon reduction of Pdx, especially in the C-terminal cluster. Residues in the C-terminal cluster (Val74, Ala76, Lys79, Ser82, and Arg104) as well as others in the vicinity of the Fe-S center (Ser7, Ala26, Ala27, Val28, and Asn30) in the reduced Pdx show a significant decrease in exchange rates relative to oxidized Pdx. This is consistent with our ^{15}N backbone dynamics results, which show that increased flexibility is observed in almost all parts of the oxidized protein, with an emphasis on the residues closer to the Fe-S center, which have also been described as a C-terminal cluster (*2, 3*). On two distinct time scales (milliseconds to hours and picoseconds to nanoseconds), oxidized Pdx has more flexibility than reduced Pdx. However, the ^{15}N dynamics results do not show significant changes in the residue 102−106 region, in contrast to the amide exchange results. This difference could be ascribed to the different time scale motions encompassed by ^{15}N dynamics and amide exchange. These techniques give information about the events on two distinct time scales, and provide a more thorough understanding of the dynamic properties. Along these lines, it is also noteworthy that nanosecond dynamics of the Trp106 studied by fluorescence experiments show different conformational states, whereas this subnanosecond motion cannot be observed for this particular residue by ^{15}N relaxation methods. Therefore, it is important to study the protein dynamics in as many different time scales as possible.

Comparison with Other Redox-Dependent Dynamics Studies. A number of groups have recently studied dynamics of redox proteins in more than one oxidation state, by using such different techniques as deuterium exchange, amide proton exchange, or ^{15}N backbone dynamics. Thioredoxin (*34, 35*), glutaredoxin (*36*), and flavodoxin (*37*) are examples of dynamics studies on reduced vs oxidized proteins without metal centers. In these cases, reduced proteins are found to be more flexible than the oxidized ones. Recently, the backbone dynamics of reduced and oxidized cytochrome b_5 were studied by ^{15}N relaxation and deuterium exchange measurements (*10*). Although it has been observed that there are minute changes between the structures of cytochrome b_5 in both oxidation states (*38*), dynamics studies indicated a more rigid system for the reduced form of cytochrome b_5. We observe the same redox sensitivity in dynamics for Pdx. Besides its various involvements in important physiological processes, cytochrome b_5 exists in a membrane-bound form in the liver, and serves as an alternate donor to P450 in the metabolism of certain xenobiotics (*39*). Cytochrome b_5 and Pdx have many differences in structure and function, the most striking difference being that cytochrome b_5 has a heme group, whereas Pdx has an Fe-S center. However, they are both electron carriers, and the similar effect of oxidation state on their backbone dynamics is noteworthy.

Calculation of Entropy Difference of Oxidized and Reduced Pdx. An upper bound for the contribution of backbone dynamics to the entropy change that occurs on oxidation of reduced Pdx to its oxidized form was calculated from eq 5 (*40*):

$$\Delta S = k\sum_{n} \ln\left(\frac{1 - S^2_{n2}}{1 - S^2_{n1}}\right) \qquad (5)$$

This equation was summed over all residues for which the order parameters were known in both oxidation states, where the initial state (state 1) is the reduced state, and the final state (state 2) is the oxidized state. Using the order parameters derived from model-free calculations for the reduced and the oxidized Pdx, we obtained an entropy contribution of 95 ± 19 J/(K·mol). The only drawback is that for rigid systems (where S^2 values are greater than 0.95), the applicability of eq 5 has been questioned (*41*). For Pdx, 37% of the observed residues in the reduced form and 17% in the oxidized form have order parameters greater than 0.95. This calculation has been done previously for cytochrome b_5 (*10*), for which the magnitude of the backbone contribution to the entropy change was found to be 70 ± 6 J/(K·mol), and only 13% of the residues have order parameters greater than 0.95. Pdx is evidently a more rigid system than cytochrome b_5. Therefore, caution should be exercised in interpreting the entropy contribution from the backbone dynamics of Pdx.

CONCLUSIONS

In this work, we have investigated the ^{15}N backbone dynamics of Pdx as a function of its redox state. Our results reveal a difference in the dynamic behavior of the reduced and the oxidized forms; the oxidized form has higher mobility in both picosecond to nanosecond and microsecond to millisecond time scales relative to the reduced form. The decrease in the protein dynamics upon reduction is observed almost everywhere in the protein. However, it is more pronounced in regions closer to the Fe-S center, especially in the C-cluster region. This decrease in protein dynamics

is in agreement with the results of a redox-dependent dynamics study by amide proton exchange.

It has been shown that reduced Pdx binds to P450cam much more readily than oxidized Pdx (*27*). Since binding of Pdx to P450cam requires some loss of degrees of conformational freedom, and since reduced Pdx is more rigid and more readily bound to P450cam in comparison with oxidized Pdx, it has been proposed that reduced Pdx populates the same conformational substates in the Pdx−P450cam complex (*42*). The decrease in the protein dynamics upon reduction of Pdx, especially in regions closer to the Fe-S center, supports this view. In particular, the drastic change in the dynamics of residue Asp34, which is implicated as a binding site for P450cam, is a very good example of this.

ACKNOWLEDGMENT

NMR experiments were carried out in the NMR Facility at the Center for Advanced Research in Biotechnology, Rockville, MD. We thank Dr. Diane Hancock and Dr. John P. Marino for assistance with pulse programs, Dr. Arthur G. Palmer III for access to Modelfree Software (Version 3.1), and Dr. Thomas C. Pochapsky for helpful discussions.

SUPPORTING INFORMATION AVAILABLE

Tables of model-free parameters for oxidized and reduced Pdx, consisting of S^2, τ_e, and R_{ex} values for many of the amino acid residues (3 pages). This material is available free of charge via the Internet at http://pubs.acs.org.

REFERENCES

1. Cushman, D. W., Tsai, R. L., and Gunsalus, I. C. (1967) *Biochem. Biophys. Res. Commun. 26*, 577−583.
2. Pochapsky, T. C., Ye, X. M., Ratnaswamy, G., and Lyons, T. A. (1994) *Biochemistry 33*, 6424−6432; Pochapsky, T. C., Jain, N. U., Kuti, M., Lyons, T. A., and Heymont, J. (1999) *Biochemistry 38*, 4681−4690.
3. Pochapsky, T. C., Ratnaswamy, G., and Patera, A. (1994) *Biochemistry 33*, 6433−6441.
4. Jain, N. U., and Pochapsky, T. C. (1998) *J. Am. Chem. Soc. 120*, 12984−12985.
5. Lyons, T. A., Ratnaswamy, G., and Pochapsky, T. C. (1996) *Protein Sci. 5*, 627−639.
6. Coxon, B., Sari, N., Holden, M. J., and Vilker, V. L. (1997) *Magn. Reson. Chem. 35*, 743−751.
7. Sari, N., Holden, M. J., Mayhew, M. P., Vilker, V. L., and Coxon, B. (1998) *Biochem. Biophys. Res. Commun. 249*, 773−780.
8. Mandel, A., Akke, M., and Palmer, A. G., III (1995) *J. Mol. Biol. 246*, 144−163.
9. Marmorino, J. L., Auld, D. S., Betz, S. F., Doyle, D. F., Young, G. B., and Pielak, G. J. (1993) *Protein Sci. 2*, 1966−1974.
10. Dangi, B., Blankman, J. I., Miller, C. J., Volkman, B. F., and Guiles, R. D. (1998) *J. Phys. Chem. B 102*, 8201−8208.
11. Grayson, D. A., Tewari, Y. B., Mayhew, M. P., Vilker, V. L., and Goldberg, R. N. (1996) *Arch. Biochem. Biophys. 332*, 239−247.
12. Kay, L. E., Torchia, D. A., and Bax, A. (1989) *Biochemistry 28*, 8972−8979.
13. Grzesiek, S., and Bax, A. (1993) *J. Am. Chem. Soc. 115*, 12593−12594.
14. Piotto, M., Saudek, V., and Sklenar, V. (1992) *J. Biomol. NMR 2*, 661−665.
15. Palmer, A. G., III, Rance, M., and Wright, P. E. (1991) *J. Am. Chem. Soc. 113*, 4371−4380.
16. Farrow, N. A., Muhandiram, R., Singer, A. U., Pascal, S. M., Kay, C. M., Gish, G., Shoelson, S. E., Pawson, T., Forman-Kay, J. D., and Kay, L. E. (1994) *Biochemistry 33*, 5984−6003.
17. Abragam, A. (1961) *Principles of Nuclear Magnetism*, Clarendon Press, Oxford.
18. Hiyama, Y., Niu, C.-H., Silverton, J. V., Bavoso, A., and Torchia, D. A. (1988) *J. Am. Chem. Soc. 110*, 2378−2383.
19. Lipari, G., and Szabo, A. (1982) *J. Am. Chem. Soc. 104*, 4546−4559.
20. Lipari, G., and Szabo, A. (1982) *J. Am. Chem. Soc. 104*, 4559−4570.
21. Clore, G. M., Driscoll, P. C., Wingfield, P. T., and Gronenborn, A. M. (1990) *Biochemistry 29*, 7387−7401.
22. Cross, T. A., and Opella, S. J. (1983) *J. Am. Chem. Soc. 105*, 306−308.
23. Kazanis, S., and Pochapsky, T. C. (1997) *J. Biomol. NMR 9*, 337−346.
24. Holden, M., Mayhew, M., Bunk, D., Roitberg, A., and Vilker, V. L. (1997) *J. Biol. Chem. 212*, 21720−21725.
25. Pochapsky, T. C., Lyons, T. A., Kazanis, S., Arakaki, T., and Ratnaswamy, G. (1996) *Biochimie (Paris) 78*, 723−733.
26. Roitberg, A. E., Holden, M. J., Mayhew, M. P., Kurnikov, I. V., Beratan, D. N., and Vilker, V. L. (1998) *J. Am. Chem. Soc. 120*, 8927−8932.
27. Davies, M. D., and Sligar, S. G. (1992) *Biochemistry 31*, 11383−11389.
28. Sligar, S. G., DeBrunner, P. G., Lipscomb, J. D., Namtvedt, M. J., and Gunsalus, I. C. (1974) *Proc. Natl. Acad. Sci. U.S.A. 71*, 3906−3910.
29. Davies, M. D., Qin, L., Beck, J. L., Suslick, K. S., Koga, H., Horiuchi, T., and Sligar, S. G. (1990) *J. Am. Chem. Soc. 112*, 7396−7398.
30. Roitberg, A. E. (1997) *Biophys. J. 73*, 2138−2148.
31. Stayton, P. S., and Sligar, S. G. (1991) *Biochemistry 30*, 1845−1851.
32. Wagner, G. (1983) *Q. Rev. Biophys. 16*, 1−57.
33. Englander, S. W., and Kallenbach, N. R. (1983) *Q. Rev. Biophys. 16*, 521−655.
34. Stone, M. J., Chandrasekhar, K., Holmgren, A., Wright, P. E., and Dyson, J. H. (1993) *Biochemistry 32*, 426−435.
35. Jeng, M.-F., and Dyson, J. H. (1995) *Biochemistry 34*, 611−619.
36. Kelley, J. J., III, Caputo, T. M., Eaton, S. F., Laue, T. M., and Bushweller, J. H. (1997) *Biochemistry 36*, 5029−5044.
37. Hrovat, A., Blumel, M., Lohr, F., Mayhew, S. G., and Ruterjans, H. (1997) *J. Biomol. NMR 10*, 53−62.
38. Dangi, B., Sarma, S., Yan, C., Banville, D. L., and Guiles, R. D. (1998) *Biochemistry 37*, 8289−8302.
39. Vergeres, G., and Waskell, L. (1995) *Biochemie 77*, 604−620.
40. Akke, M., Brüschweiler, R., and Palmer, A. G., III (1993) *J. Am. Chem. Soc. 115*, 9832−9833.
41. Yang, D., and Kay, L. E. (1996) *J. Mol. Biol. 263*, 369−382.
42. Pochapsky, T. C., Arakaki, T., Jain, N., Kazanis, S., Lyons, T. A., Mo, H., Patera, A., Ratnaswamy, G., and Ye, X. (1998) *Structure, Motion, Interaction and Expression of Biological Macromolecules*, Proceedings of the Tenth Conversation (1997) State University of New York, Albany, NY (Sarma, R. H., and Sarma, M. H., Eds.) pp 79−84, Adenine Press, New York.

BI9906423